Composites Part B 147 (2018) 114–121

Contents lists available at ScienceDirect

Composites Part B

journal homepage: www.elsevier.com/locate/compositesb

Determination of adhesion strength of pre-bond contaminated composite-to-metal bonded joints by centrifuge tests

M. Hoffmann[a], K. Tserpes[b,*], E. Moutsompegka[b], M. Schlag[a], K. Brune[a]

[a] Fraunhofer Institute for Manufacturing Technologies and Advanced Materials, Wiener Str. 12, 28359, Bremen, Germany
[b] Laboratory of Technology & Strength of Materials, Department of Mechanical Engineering & Aeronautics, University of Patras, Patras, 26500, Greece

ARTICLE INFO

Keywords:
Composite bonded joints
Pre-bond contamination
Centrifuge testing
Adhesion strength
Kissing bonds

ABSTRACT

In the present work, the effect of pre-bond contamination scenarios related to production and repair processes on the adhesion strength of composite-to-metal joints is investigated by means of the novel centrifuge testing technology. The composite substrates have been subjected to contamination with release agent, moisture, fingerprint, thermal degradation and de-icing fluid before being bonded on the metallic stamp. Different contamination levels have been considered for each scenario. The standard deviation of adhesion strength values differs for each sample category and in some cases, is relatively high. The experimental results show a considerable decrease of adhesion strength for all contamination scenarios. The evaluation of the adhesion strength values is assisted by the characterization of the failure modes. In most cases, the transition between the failure modes explains the variation of adhesion strength. By taking into advantage the simplicity of the experimental process, numerous tests have been conducted within a very short time. Based on the practicality of the experimental process and the validity of the findings, it can be concluded that the centrifuge testing technology can be potentially used as a reliable testing method for the characterization of bonded joints.

1. Introduction

In the last two decades, adhesive joining finds an increasing use in many industries due to the advantages it provides over the conventional structural joining methods (e.g. mechanical fastening). In aerostructures, adhesive bonding is applied in metal-to-metal joints, composite-to-composite joints and composite-to-metal joints both for assembling parts and for patch-repairing. However, application of adhesive bonding in aerostructures is limited for the moment to secondary structural parts that are not load-critical [1,2] due to certification reasons. In the certification requirements for primary composite aircraft structures, it is stated that for bonded joints *repeatable and reliable non-destructive inspection techniques (NDI) must be established that ensure the strength of each joint* [3]. Repeatable and reliable NDI techniques for ensuring strength of bonded joints are required for both the installation phase to check the physicochemical conditions of the bonded surfaces and the in-service phase to monitor the integrity of the joints and support structural health monitoring systems. While conventional NDI techniques, such as the ultrasounds have been proved reliable in the detection of debonding, for the detection of kissing bonds, new techniques of extended capabilities need to be developed [1,4].

Although joint configurations are designed so as to transfer the load between the assembled parts through pure shear, during operation, normal stresses are also usually developed. The most effective and frequently used method for providing quantitative results in terms of normal force per area is the standardized pull-off test which quantifies adhesion strength by means of tension [5]. The standardized conventional adhesion tests are characterized by a series of drawbacks: they are single-sample tests and time-consuming, a two-sided clamping of the samples is required [6,7] and shear stresses are also developed due to sample misalignment [8]. In the last few years, a novel test method, based on the principle of the centrifuge force, has been proposed for measuring adhesion strength of adhesive joints. The principle of centrifuge force has been used for many years as the main mechanical separation process for solids from liquids or for liquids from liquids [9,10] in various applications, e.g. food industry [11], bioengineering [12], ice removal on ground and air transportation industry [13], etc. The centrifuge test is a multi-sample, single-lap fast test. The application of the centrifuge test on adhesive joints is still very new and under evaluation. Only three works have been reported in the area. Rietz et al. [14] have used the centrifuge test to determine the tensile and shear strength of metal-to-metal adhesive bonded joints, while Beck et al. [5,15] have investigated the tensile strength of various optical coatings

* Corresponding author.
E-mail address: kitserpes@upatras.gr (K. Tserpes).

https://doi.org/10.1016/j.compositesb.2018.04.014
Received 3 December 2017; Received in revised form 21 March 2018; Accepted 5 April 2018
Available online 06 April 2018
1359-8368/

and adhesive films using steel and glass substrates.

In a series of works published by the authors [1,2,16,17], it has been found by means of Mode-I and Mode-II fracture toughness tests, that kissing bonds created by production- and repair-related contamination scenarios, might degrade significantly the fracture toughness of composite bonded joints. Additionally, the joint strength of contaminated adhesively bonded joints has been studied with conventional testing methods indicating the detrimental effect of the contaminant [18–20]. However, the effect of such contamination scenarios on adhesion strength of the bonded joints utilizing the centrifuge test has not been studied previously. In the present work, a similar study has been conducted using centrifuge tests in order from one hand to evaluate this novel testing method for CFRP-to-metal adhesive joints and on the other hand to evaluate the effect of contamination on the adhesion (pull-out) strength of the joints. The production-related pre-bond contamination scenarios considered are the release agent, the moisture and the fingerprint and the repair-related scenarios are the fingerprint, the thermal degradation and the de-icing fluid.

2. Pre-bond contamination of CFRPs

Adhesive bonding is used by the aircraft industry both for assembling composite structural parts and for implementing composite patch repairs in damaged structural parts. In both applications, several pre-bond surface contamination scenarios that could affect the bonding quality are possible to occur. In this work, three contamination scenarios related to the production process and three contamination scenarios related to the repair process have been considered.

During the molding process of the composite panels, silicone (Si)-based release agents are used to facilitate easy removal of the part from the mold. Si-contamination on the CFRP surface caused by release agent residuals hinders the adhesion of the adhesive onto the substrate [16,17].

Pre-bond moisture penetration into the composite adherend can occur either via air humidity or via direct contact with liquid water. CFRP panels undergo several pre-treatment procedures, such as wet abrasion and the water brake test to ensure the effectiveness of the cleaning procedure [16,17]. Although precaution measures are implemented, such as large autoclaves to remove moisture by heat-drying, the problem persists. Moisture uptake mainly affects the properties of the matrix resulting to swelling and to the development of stresses large enough to pull the matrix away from the fiber [16–18]. Moreover, moisture affects the adhesion properties [21].

Contamination by fingerprints can occur due to inadequate cleaning of the bonding surfaces or inappropriate handling after the cleaning process [22,23]. It may occur during both the production and repair processes. Fingerprint contamination leads to the formation of thin contaminant films on the bonding surfaces and finally, to lower adhesion quality [23].

During service, CFRP aircraft parts may be exposed to high temperatures, e.g. the fuselage parts stroked by lightning [24] causing local overheating and damage of the matrix or the wing parts which are close to the engines. Besides the loss in the mechanical properties of the structural parts, thermal degradation of the CFRP parts might also affect bonding in a repair.

In winter, airports use de-icer to maximize the runway friction during plane taxiing. Runway de-icing fluid is one of the most commonly encountered fluids that aircraft structures may be exposed to, as it can be swirled from the runway to outer parts of the aircraft [2]. During patch-repairing of composite parts, inadequate cleaning can result to de-icing fluid remains. After drying, the potassium formiate, which is present in the de-icing fluid, forms a thin layer on the CFRP part, thus hindering the bonding quality.

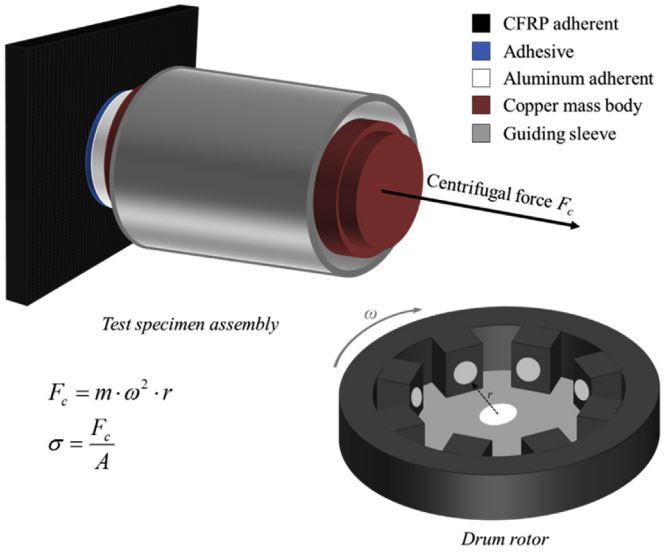

Fig. 1. Measurement principle of the centrifuge test.

3. The centrifuge testing principle

The centrifuge test is based on the physical law of inertia of a body [14]. Due to rotation, a progressively increasing radial centrifugal force is applied to the specimen being tested. The load increase is adjusted by the variation of the rotor's rotational speed. The centrifuge testing principle for the bonded joints is illustrated in the schematic of Fig. 1. The specimen comprises a composite plate (adherend) bonded to a metallic cylindrical stamp. The axial centrifugal force acts as a normal tensile force in the bondline. If the applied load exceeds the tensile strength of the joint, rupture occurs, and the test stamp changes its position within the guiding sleeve. The detachment of the test stamp from the CFRP adherend at the time of rupture is automatically detected and a position-coded signal is sent out of the turning rotor transmitting the current rotor speed as well as rupture time [25].

The centrifugal force F_c (N) is derived from:

$$F_c = m \cdot \omega^2 \cdot r \quad (1)$$

where m (kg) is the mass of the stamp, r (m) is the distance of the test stamp to the rotational axis and ω (rad/s) is the angular velocity related to frequency ν by:

$$\omega = 2 \cdot \pi \cdot \nu \quad (2)$$

Dividing the centrifugal force F_c by the area of the bondline A (mm^2), the tensile adhesion strength σ (MPa) is derived

$$\sigma = \frac{F_c}{A} \quad (3)$$

4. Experimental

4.1. Materials and specimen preparation

4.1.1. CFRP adherends

The specimens used in the centrifuge tests had a stamp-to-plate configuration (Fig. 2). The CFRP adherends were manufactured from the M21E/IMA prepreg material. The lay-up sequence of the panels was $[(0/90/45/-45)_3]_s$. The lay-up of the plies was applied by an automated tape laying equipment. For the preparation of the CFRP adherends, the panels were cleaned with isopropanol (IPA)-soaked tissues to remove part of the release agent and any other soluble contamination, followed by a slight grinding step of the surfaces to remove residual release agent that had penetrated or was incorporated into the topmost resin layers. After wiping the samples with demineralized water and then with IPA

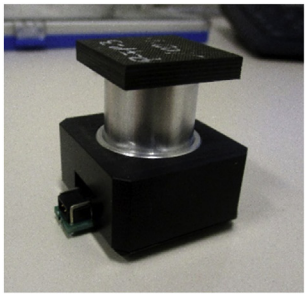
(a)

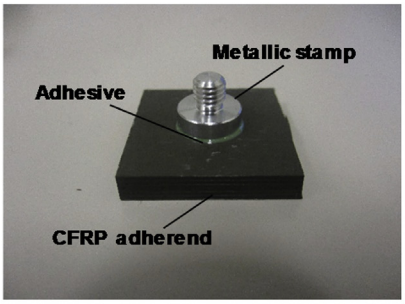

(b)

Fig. 2. The stamp-to-plate specimen used in the centrifuge tests (a) complete specimen and (b) metallic stamp bonded to the CFRP adherend.

to remove the dust from grinding and residual silicone, a second grinding step, followed by wiping off the dust with demineralized water and IPA was applied. The samples were cut into the desired size by dry diamond cutting. The final dimensions of the CFRP adherends are 25 mm × 25 mm x 4.4 mm. After the cleaning, the surface of the composite adherends was either left clean (reference) or purposely contaminated before bonding.

4.1.2. Test stamp

The modular test stamps bonded to the CFRP adherends consist of the aluminum (EN AW-2007) adherend screwed onto a mass body made of copper (see Fig. 1). The test stamps had a diameter of 10 mm on the bonding face and were anodized in phosphoric-sulfuric acid (PSA, 120 g/l H_3PO_4/80 g/l H_2SO_4). Prior to anodizing, all specimens were de-greased (Turco 4215 NC from Henkel), etched (Aluminetch No. 2 from Henkel) and pickled (Turco Liquid Smutgo NC from Henkel).

4.1.3. Bonding of the samples

For the bonding of the samples, the film adhesive was hole-punched to a diameter of 10 mm and then deposited onto the test stamp (cleaned by sonication for 5 min in IPA) which was then placed onto the CFRP sample. The production samples bonded with the FM300K adhesive were cured in an autoclave using a custom-made curing device at 3 bars and 175 °C for 60 min (heat up to 175 °C in 60 min, cool down to room temperature in 60 min). The repair samples bonded with FM300-2 adhesive were cured at 2 bars and 121 °C for 90 min (heat up to 121 °C in 30 min, cool down to room temperature in 60 min).

4.1.4. Production-related contamination

All contaminations were applied to cleaned surfaces. The release agent (RA) FREKOTE 700NC was dissolved and diluted in heptane (1, 2, and 4 vol% solutions) and applied to the adherends by dip coating. The resultant concentrations of release agent on the surfaces in terms of Si are listed in Table 1. Moisture (MO) contamination was applied by first drying the samples in an oven at 80 °C and then exposing them to humidity conditions at 70 °C for two weeks. The different humidity conditions and the respective labeling of the MO-contaminated samples are depicted in Table 2. In the production-related scenario, fingerprint (FP) contamination was applied using a standardized salty fingerprint solution (artificial hand perspiration solution) according to the DIN ISO 9022-12 [26] standard. The solution contained sodium chloride, urea, ammonium chloride, lactic acid, acetic acid, pyruvic acid and butyric acid in demineralized water. Samples were prepared by applying this solution with the size of a fingerprint to the samples. Different degrees of contamination were achieved by using different dilutions of the FP solution (10, 50 and 100 vol% solutions). The resultant concentrations of the sodium chloride chemical elements on the CFRP adherends for the production-related FP-contamination scenario are given in Table 3.

Table 1
Labeling of release agent-contaminated samples (letter P refers to Production).

Sample category	Si, at%
P-RA-1	3.2 ± 1.0
P-RA-2	5.1 ± 0.7
P-RA-3	6.2 ± 0.3

Table 2
Labeling of moisture-contaminated samples (letter P refers to Production).

Sample category	Humidity conditions
P-MO-1	30%RH
P-MO-2	75%RH
P-MO-3	98%RH

4.1.5. Repair-related contamination

In the repair-related scenario, fingerprint (FP) contamination was applied using the Skydrol 500B-4 hydraulic-oil from Eastman. Skydrol fingerprints were applied to the surfaces using a plastic finger and different concentrations of Skydrol in heptane. The labeling of the FP-contaminated samples for the repair-related scenario is given in Table 4. Thermal degradation (TD) was carried out in an oven with air circulation. The samples were placed inside the oven at stage temperature and were subjected to the heating phase. The specimens stayed inside the oven for 2 h after the indicated temperature was reached. The applied temperature values and the respective labeling of the specimens are given in Table 5. The de-icer (DI) used was the SAFEWAY KF from CLARIANT. It was diluted with demineralized water to obtain solutions (2, 7, and 10 vol% DI) with different concentrations of potassium. The de-icer was applied on the surfaces by dip coating (aqueous solution) and then dried in the oven for 2 h at 40 °C. Then, acclimatization at room temperature was allowed for at least for 24 h. Labeling of the DI-contaminated samples is given in Table 6.

4.2. Centrifuge tests

The centrifuge tests were carried out using a LUMiFrac desktop adhesion analyzer equipped with a LSFR-ST: 200.42 drum rotor of up to eight testing units (Fig. 3). The fully loaded rotor allows for a maximum rotational speed ω of 13,000 rpm corresponding to a centrifugal acceleration of 13,715 g [25].

During the preparation of the specimens and the test, the test stamp

Table 3
Labeling of fingerprint-contaminated samples (letter P refers to Production).

Sample category	Contamination solution	
	at% Na	at% Cl
P-FP-1	0.2 ± 0.1	0.5 ± 0.3
P-FP-2	0.5 ± 0.1	0.9 ± 0.0
P-FP-3	0.7 ± 0.1	1.1 ± 0.2

Table 4
Labeling of fingerprint-contaminated samples (letter R refers to Repair).

Sample category	Contamination solution
R-FP-1	20% Skydrol in heptane
R-FP-2	50% Skydrol in heptane
R-FP-3	100% Skydrol (no dilution)

Table 5
Labeling of the thermally degraded samples (letter R refers to Repair).

Sample category	Applied temperature
R-TD-1	220 °C
R-TD-2	260 °C
R-TD-3	280 °C

Table 6
Labeling of the samples degraded by the de-icer (letter R refers to Repair).

Sample category	K, at%
R-DI-1	6.4 ± 1.8
R-DI-2	10.9 ± 2.3
R-DI-3	12.0 ± 1.4

was supported within the testing unit by means of a guiding sleeve (Fig. 1) to avoid the development of shear forces at both processes [5,15]. The test specimens were inserted into the detection modules and afterwards the loaded modules into the drum rotor by an easy plug-in procedure. By means of the SEPView software, the desired load-controlled testing sequence was realized. To achieve compatibility with conventional testing machines (in load-controlled mode), the increase in the rotational speed of the rotor was designed to be quadratic. According to Eq. (1), a square root-like increase in the rotational speed is accompanied by a linear increase in the centrifugal force [15]. Then, the rotor and centrifuge lid were closed and the testing procedure was initiated. Six specimens per contamination scenario were tested. The duration of each testing was from 6 to 20 s on average depending on the contamination scenario. The rupture event was detected on-line outside the drum rotor using a position-coded and rpm-correlated data transmission from the inside of the testing units mounted in the drum rotor. The current rotor speed and rupture time are transmitted and the centrifugal force F_c (N) was calculated using Eq. (1).

4.3. Failure characterization

After testing, high resolution microscope images of the failure surfaces of both the CFRP adherend and the test stamp side were taken and examined aiming to characterize the failure patterns. The main failure modes observed are schematically described in Fig. 4. Adhesive (ADH) failure occurs when the separation takes place at the adhesive/adherend interface, cohesive (CO) failure when the separation takes place within the adhesive, fiber-tear (FT) failure when the failure occurs exclusively within the matrix resulting in the appearance of fibers on both ruptured surfaces and light-fiber-tear (LFT) failure when failure occurs within the adherend, near the interface characterized by a thin layer of the matrix on the surface with few or no fibers transferred from the substrate to the adhesive and thin-layer cohesive (TLC) failure when the separation takes place within the adhesive but not at the mid-thickness.

The classification, identification and characterization of the failure modes of the joints were conducted according to the ASTM D5573 [27] standard by using the photographic guidelines shown in Fig. 7. For increased accuracy, a grid drawn on a clear film placed over the failure surface was used and the squares of each type of failure mode were counted providing the input for the percentage calculation.

5. Results and discussion

Figs. 5 and 6 display the average adhesion strength values, as derived from Eq. (3), for the production-related and the repair-related samples, respectively. In the bar-charts, the average adhesion strength values of the respective reference samples and the standard deviation ranges for each case are also included.

Fig. 7 depicts representative microscope photos of the different failure modes from various samples while Figs. 8–13 display the average surface percentages of the failure modes for the different contamination scenarios. The reference specimens for both categories (production and repair) failed in ADH and LFT failure modes. The adhesive mainly remained on the metallic stamp which is an indication for a stronger bond between the metallic stamp and the adhesive. This stands for all cases of adhesive failure. On the other hand, the considerable percentage of LFT failure mode (~30%) is also an indication for a strong bond between the CFRP and the adhesive. The P-REF samples showed a much higher (almost double) adhesion strength than the R-REF samples which is due to the different type of adhesive used and the different curing conditions applied.

For the P-RA scenario, the presence of release agent leads to the decrease of adhesion strength at the same level for P-RA-1 and P-RA-2 cases and at a lower level for the P-RA-3 case. This finding agrees with the findings of [1]. Regarding the failure modes (Fig. 8), there is an increase of ADH failure and a decrease of LFT failure. This transition is due to the weakening of the adherend/adhesive bond. However, a safe conclusion about the effect of contamination level on the failure modes cannot be drawn from the variation of the average percentages of the failure mode.

For the P-MO scenario, the results show that the moisture absorption by the CFRP adherend causes a decrease of adhesion strength at the same level for P-MO-1 and P-MO-2 and at a lower level for P-MO-3. Observation of Fig. 9 reveals that moisture absorption leads to the

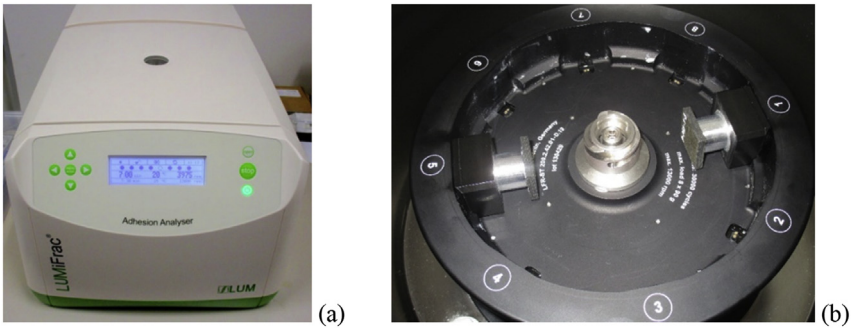

(a) (b)

Fig. 3. (a) The LUMiFrac desktop analyzer, (b) stamp-to-plate test specimens inside the drum rotor.

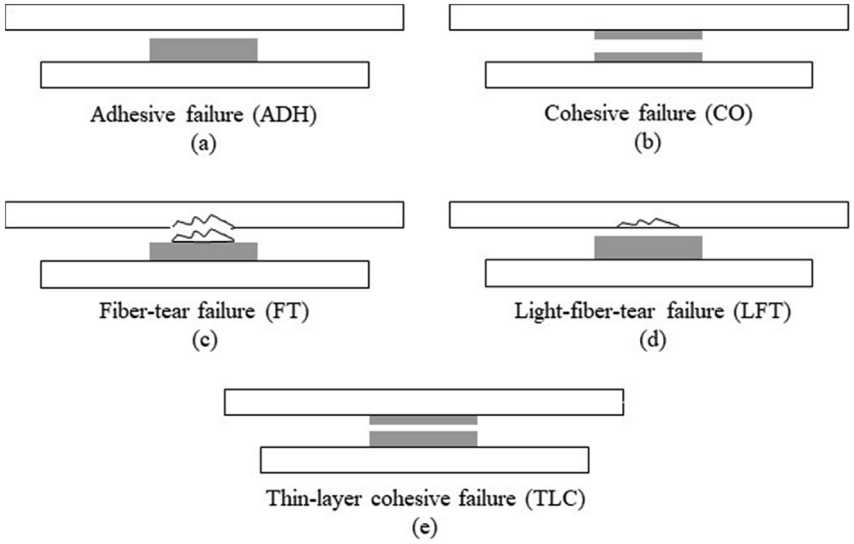

Fig. 4. Schematic representation of the basic failure modes observed in the present study.

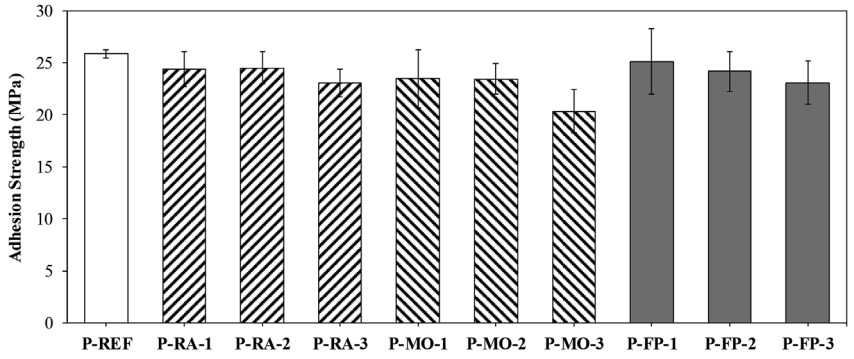

Fig. 5. Average adhesion strength values for the production-related sample categories.

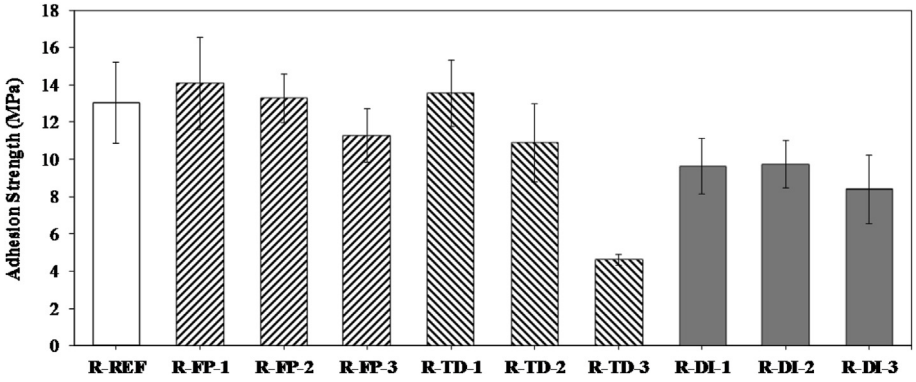

Fig. 6. Average adhesion strength values for the repair-related sample categories.

increase of ADH failure and to the decrease of LFT failure mode. This is an indication for the weakening of the CFRP/adhesive bond due to presence of moisture on the CFRP's surface.

Similar conclusions are drawn for the P-FP scenario for both the adhesion strength and the type and percentage of the failure modes. However, the large deviation of the P-FP-1 and P-FP-2 cases, which lies within the limits of the P-REF values, hinders the indication of a definite conclusion regarding these contamination levels. The only difference between the P-MO and the P-FP scenarios is that the decrease of adhesion strength is smaller for the P-FP scenario (Fig. 5).

For the Skydrol-based R-FP scenario, there seems to be an increase of adhesion strength for the R-FP-1 case, a no variation of adhesion strength for the R-FP-2 case and a decrease of adhesion strength for the R-FP-3 case. However, a safe conclusion for the R-FP1-1 and R-FP-2 cases cannot be drawn due to the very high standard deviation of the results for these two cases and the R-REF case. For the R-FP-3 case, there is a considerable decrease of adhesion strength. On the other hand, the percentage of the failure modes in Fig. 11 reveals a similar failure behavior for the R-FP-1 case and for the R-FP-2 and the R-FP-3 cases, a decrease of LFT failure and an increase of ADH and TLC failure modes. The increase of the ADH failure mode in the R-FP-3 case agrees with the considerable decrease of the adhesion strength of the R-FP-3 specimens, as ADH failure mode is an indication of a weak bond. The fact that three failure modes occur in the R-FP scenario is closely related

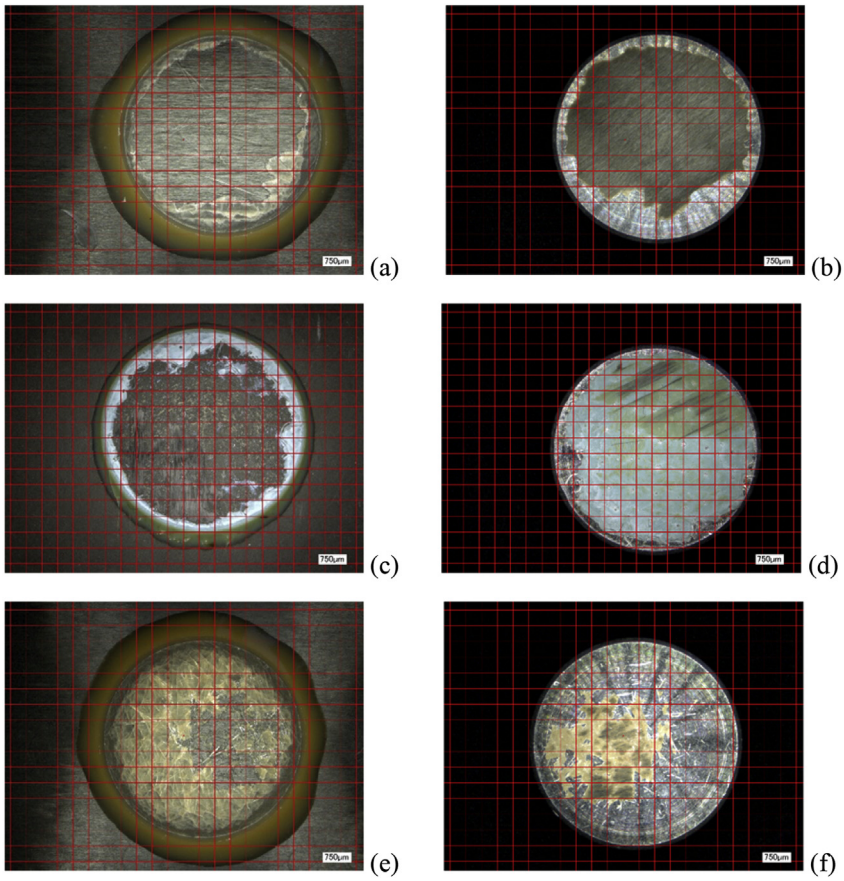

Fig. 7. Representative microscope photos of the different failure modes: (a) ADH + FT for R-TD sample (CFRP's side), (b) ADH + FT for R-TD sample (stamp's side), (c) ADH + LFT for P-MO sample (CFRP's side), (d) ADH + LFT for P-MO sample (stamp's side), (e) ADH + FT + TLC for R-DI sample (CFRP's side), (f) ADH + FT + TLC for R-DI sample (stamp's side).

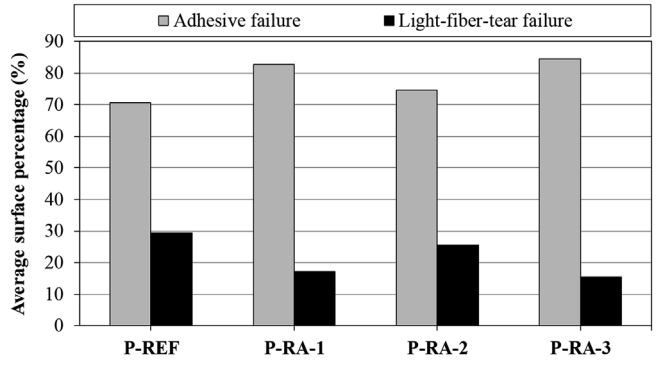

Fig. 8. Average surface percentage of the different failure modes for the P-RA samples.

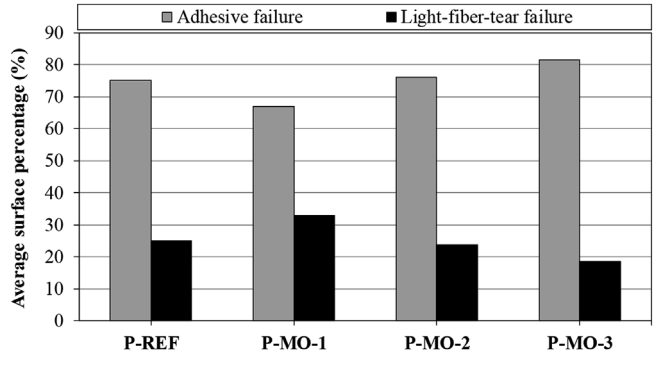

Fig. 9. Average surface percentage of the different failure modes for the P-MO samples.

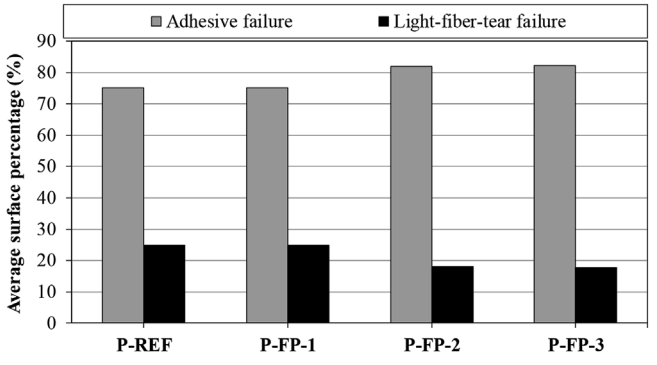

Fig. 10. Average surface percentage of the different failure modes for the P-FP samples.

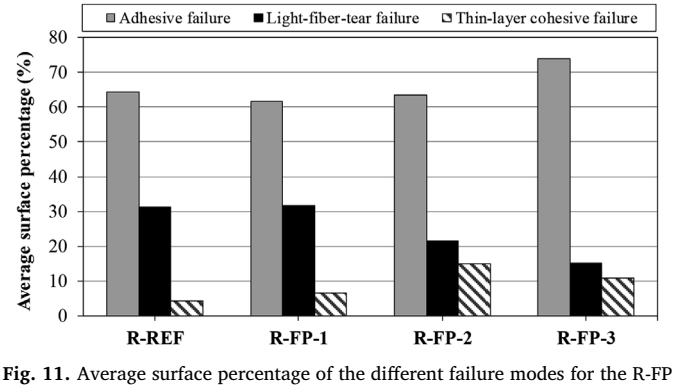

Fig. 11. Average surface percentage of the different failure modes for the R-FP samples.

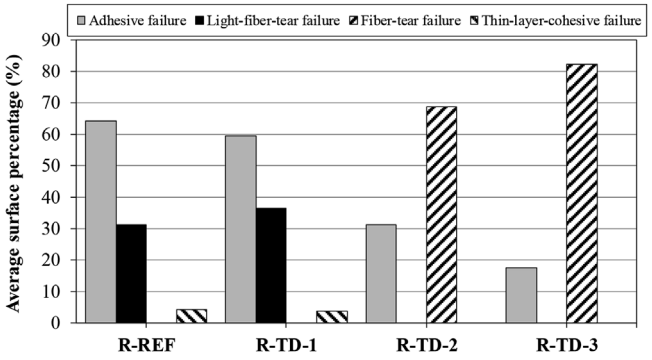

Fig. 12. Average surface percentage of the different failure modes for the R-TD samples.

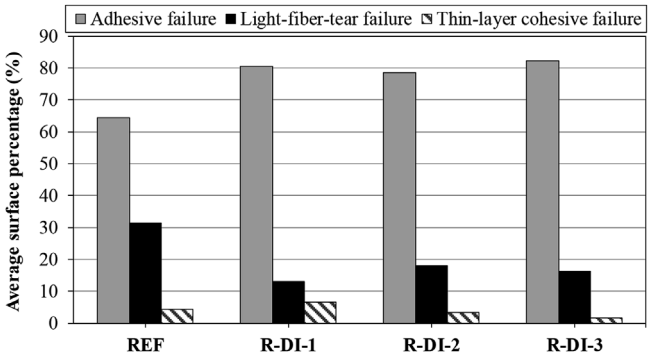

Fig. 13. Average surface percentage of the different failure modes for the R-DI samples.

to the large standard deviation of the adhesion strength values and makes it very difficult to clearly evaluate the effect of the different FP contamination concentrations. The large standard deviation of the results of the R-FP scenario could be attributed to the use of Skydrol for the application of FP contamination. The use of a dip coating contamination might lead to a smaller standard deviation.

For the R-TD scenario, the R-TD-1 case presents a similar behavior both in terms of adhesion strength and failure modes (ADH and LFT and TLC, see Fig. 12) with the R-REF case. However, there is evidence of adhesion strength improvement for the case of the low temperature. Thermal degradation results in the thermo-oxidation of the resin [16,24]. Depending on the temperature level applied, this may either lead to the improvement of the resin performance due to the presence of carboxyl bonds or cause the development of an oxidized layer which hinders the adhesion at the surface of the CFRP substrate [16]. On the contrary, the R-TD-2 and R-TD-3 cases present a lower adhesion strength and different failure modes (ADH and FT, see Fig. 12). In the latter cases, the decrease of adhesion strength is attributed to the degradation of the polymer matrix in the first layer of the CFRP adherend because of the increased temperature, which causes a FT failure mode. Indeed, as shown in Fig. 12, FT failure increases drastically as the temperature increases.

Finally, for the R-DI scenario, there is a detrimental effect of the presence of de-icer on the adhesion strength of the joint. Specifically, for the R-DI-1 and R-DI-2 cases, there is a 25% reduction of adhesion strength, while the reduction for the R-DI-3 the reduction is almost 36%. The failure modes percentages (Fig. 13) show that the increase of the DI concentration causes an increase of ADH failure mode, due to the formation of thin layer by the de-icer which acts as a barrier in the bonding of the adhesive and the CFRP adherend. However, in contrast with the adhesion strength, there is not a clear differentiation regarding the failure mode percentages between the different de-icer concentrations.

6. Conclusions

In the present work, the effect of pre-bond contamination scenarios related to production and repair processes on the adhesion strength of composite-to-metal joints has been investigated by means of the novel centrifuge testing technology.

From the evaluation of the experimental results, the following conclusions can be drawn:

- The production related contamination scenarios tend to decrease the adhesion strength with the high level of contamination being the most detrimental for all the cases. The lower adhesion strength has been measured for the P-MO-3 case (98% RH). The standard deviation is also considerable but within acceptable limits.
- The values of adhesion strength for the R-REF samples present a high standard deviation which is due to the different adhesive used and the different curing conditions applied. In all repair-related contamination scenarios, except for the R-FP-1 and R-TD-1, there is a decrease of the adhesion strength. The lower adhesion strength for this set of scenarios has been measured for the P-TD-3 case (280°C).

From the experimental process, it can be concluded that the centrifuge testing technology shows a great potential to be established as a test method for the characterization of pristine and defected bonded joints as it is a fast testing process which generates repeatable tests capable of describing the strength of the joints.

Acknowledgements

The research leading to these results has received funding from the European Union's Horizon 2020 research and innovation program under grant agreement n° 636494 (Project ComBoNDT: Quality Assurance Concepts for Adhesive Bonding of Aircraft Composite Structures by Extended NDT).

References

[1] Markatos DN, Tserpes KI, Rau E, Brune K, Pantelakis Sp. Degradation of mode-I fracture toughness of CFRP bonded joints due to release agent and moisture pre-bond contamination. J Adhes 2014;90:156–73. http://dx.doi.org/10.1080/00218464.2013.770720.
[2] Moutsompegka E, Tserpes KI, Polydoropoulou P, et al. Experimental study of the effect of pre-bond contamination with de-icing fluid and ageing on the fracture toughness of composite bonded joints. Fatig Fract Eng Mater Struct 2017;40:1581–91. http://dx.doi.org/10.1111/ffe.12660.
[3] Code of Federal Regulations. Federal Aviation Administration, 14 C.F.R § 23.573 Damage tolerance and fatigue evaluation of structure. 2011.
[4] Rokhlin SI, Lavrentyev AI, Li B. Ultrasonic evaluation of environmental durability of adhesive joints. Res Nondestr Eval 1993;5:95–109. https://doi.org/10.1007/BF01606359.
[5] Beck U, Hielscher S, Weise M, Mix R, Lerche D, Rietz U. Progress in quantitative adhesion testing of films and coatings by means of centrifuge technology – present state of the art. PSE 2012-13th int. Conf. Plasma surf. Eng., garmisch-partenkirchen, Germany. 2012. p. 169–72.
[6] DIN EN 15870: 2009–08. Adhesives - determination of the tensile strength of stump adhesives. German Institute for Standardization; 2009.
[7] ISO 4624:2002. Paints and varnishes – pull-off test for adhesion. International Organization for Standardization; 2002.
[8] Beck U, Hielscher S, Mix R, Weise M, Lerche D, Rietz U. Comparative determination of the adhesion and adhesive strength of modified plastic surfaces: centrifugal technology and conventional test methods. IKV - Institute of Plastics Processing in Industry and the Skilled Crafts at RWTH Aachen University; 2012.
[9] Sutherland K. Filtration and separation technology: what's new with centrifuges? Filtr Sep 2009;46:30–2. http://dx.doi.org/10.1016/S0015-1882(09)70126-0.
[10] Schulze HJ, Wahl B, Gottschalk G. Determination of adhesive strength of particles within the liquid/gas interface in flotation by means of a centrifuge method. J Colloid Interface Sci 1989;128:57–65. http://dx.doi.org/10.1016/0021-9797(89)90384-6.
[11] Liu Z, Carroll ZS, Long SC, Roa-Espinosa A, Runge T. Centrifuge separation effect on bacterial indicator reduction in dairy manure. J Environ Manag 2017;191:268–74. http://dx.doi.org/10.1016/j.jenvman.2017.01.022.
[12] Hagerman E, Shim J, Gupta V, Wu B. Evaluation of laser spallation as a technique for measurement of cell adhesion strength. J Biomed Mater Res 2007;82:852–60. http://dx.doi.org/10.1002/jbm.a.31011.

[13] Laforte C, Beisswenger A. Icephobic material centrifuge adhesion test. 11th international workshop on atmospheric icing of structures (IWAIS XI), montreal, CA. 2005.
[14] Rietz U, Lerche D, Hielscher S, Beck U. Centrifugal adhesion testing technology (CATT) - a valuable tool for strength determination. J Adhes Soc Japan 2015;51:293–7. http://dx.doi.org/10.11618/adhesion.51.293.
[15] Beck U, Reiners G, Lerche D, Rietz U, Niederwald H. Quantitative adhesion testing of optical coatings by means of centrifuge technology. Surf Coating Technol 2011;205:S182–6. http://dx.doi.org/10.1016/j.surfcoat.2010.07.045.
[16] Markatos DN, Tserpes KI, Rau E, Markus S, Ehrhart B, Pantelakis S. The effects of manufacturing-induced and in-service related bonding quality reduction on the mode-I fracture toughness of composite bonded joints for aeronautical use. Compos B Eng 2013;45:556–64. http://dx.doi.org/10.1016/j.compositesb.2012.05.052.
[17] Pantelakis S, Tserpes KI. Adhesive bonding of composite aircraft structures: challenges and recent developments. Sci China Phys Mech Astron 2014;57:2–11. http://dx.doi.org/10.1007/s11433-013-5274-3.
[18] Jeenjitkaew C, Luklinska Z, Guild F. Morphology and surface chemistry of kissing bonds in adhesive joints produced by surface contamination. Int J Adhesion Adhes 2010;30:643–53. http://dx.doi.org/10.1016/j.ijadhadh.2010.06.005.
[19] Sugita Y, Winkelmann C, Saponara V La. Environmental and chemical degradation of carbon/epoxy lap joints for aerospace applications, and effects on their mechanical performance. Compos Sci Technol 2010;70:829–39. http://dx.doi.org/10.1016/j.compscitech.2010.01.021.
[20] Doyle G, Pethrick RA. Environmental effects on the ageing of epoxy adhesive joints. Int J Adhesion Adhes 2009;29:77–90. http://dx.doi.org/10.1016/j.ijadhadh.2008.02.001.
[21] Budhe S, Banea MD, de Barros S, da Silva LFM. An updated review of adhesively bonded joints in composite materials. Int J Adhesion Adhes 2017;72:30–42. http://dx.doi.org/10.1016/j.ijadhadh.2016.10.010.
[22] Creemers F, Geurts KJ, Noeske M. Influence of surface contaminations on the quality and bond strength of structural adhesive joints. Eur. Adhes. Conf, United Kingdom 2016:405–8.
[23] Gause RL. A noncontacting scanning photoelectron emission technique for bonding surface cleanliness inspection. NASA marshall space flight center. Presented at the fifth annual NASA NDE workshop, Cocoa Beach, FL. 1987.
[24] Tserpes KI, Markatos DN, Brune, Hoffmann M, Rau E, Pantelakis Sp. A detailed experimental study of the effects of pre bond contamination with a hydraulic fluid thermal degradation and poor curing on fracture. J Adhes Sci Technol 2014;28:1865–80. http://dx.doi.org/10.1080/01694243.2014.925387.
[25] GmbH LUM. Technical specification of adhesion analyser LUMiFrac Available at http://www.lumifrac.com.
[26] DIN ISO 9022–12. Optics and photonics – environmental test methods – Part 12: Contamination. International Organization for Standardization; 2012.
[27] ASTM D5573-99(2005). Standard practice for classifying failure modes in fiber-reinforced-plastic (FRP) joints. West Conshohocken, PA: ASTM International; 2005www.astm.org.